AGU PUBLICATIONS

Geochemistry, Geophysics, Geosystems

TECHNICAL REPORTS: METHODS

10.1002/2014GC005631

Key Points:
- The PRIMELT3 MEGA.xlsm software supersedes PRIMELT2.xls
- Uncertainties in derived temperatures are quantified
- A computed anhydrous peridotite solidus is obtained that agrees well with experimental constraints

Supporting Information:
- Readme
- PRIMELT3 MEGA.xlsm

Correspondence to:
C. Herzberg,
herzberg@rci.rutgers.edu

Citation:
Herzberg, C., and P. D. Asimow (2015), PRIMELT3 MEGA.XLSM software for primary magma calculation: Peridotite primary magma MgO contents from the liquidus to the solidus, *Geochem. Geophys. Geosyst.*, *16*, 563–578, doi:10.1002/2014GC005631.

Received 23 OCT 2014
Accepted 29 JAN 2015
Accepted article online 5 FEB 2015
Published online 26 FEB 2015

PRIMELT3 MEGA.XLSM software for primary magma calculation: Peridotite primary magma MgO contents from the liquidus to the solidus

C. Herzberg[1] and P. D. Asimow[2]

[1]Department of Earth and Planetary Sciences, Rutgers University, Piscataway, New Jersey, USA, [2]Department of Geological and Planetary Sciences, California Institute of Technology, Pasadena, California, USA

Abstract An upgrade of the PRIMELT algorithm for calculating primary magma composition is given together with its implementation in PRIMELT3 MEGA.xlsm software. It supersedes PRIMELT2.xls in correcting minor mistakes in melt fraction and computed Ni content of olivine, it identifies residuum mineralogy, and it provides a thorough analysis of uncertainties in mantle potential temperature and olivine liquidus temperature. The uncertainty analysis was made tractable by the computation of olivine liquidus temperatures as functions of pressure and partial melt MgO content between the liquidus and solidus. We present a computed anhydrous peridotite solidus in T-P space using relations amongst MgO, T and P along the solidus; it compares well with experiments on the solidus. Results of the application of PRIMELT3 to a wide range of basalts shows that the mantle sources of ocean islands and large igneous provinces were hotter than oceanic spreading centers, consistent with earlier studies and expectations of the mantle plume model.

1. Introduction

Basalts, high-MgO picrite melts and komatiites that have erupted on Earth were produced by variable conditions of partial melting of a mantle source and partial crystallization, assimilation, and mixing during transit to and within the crust. If the effects of partial melting can be isolated, then it is possible to use their compositions to distinguish hot from cold mantle sources, which is important in understanding the thermal characteristics of ambient and anomalous mantle [*Herzberg et al*., 2007; *Putirka et al*., 2007; *Lee et al*., 2009]. However, extracting this information from a lava is not straightforward because primary magmas that form by partial melting of a mantle source are transformed by partial crystallization, assimilation, and mixing during transit to the crust [*O'Hara*, 1968]. This is the primary magma problem in mantle petrology.

A forward model is a petrological method for computing how the chemistry of melts change from the beginning of melt production at depth in the mantle to solidification in the crust. Melts in the mantle can respond to variations in temperature (T) and pressure (P) of melting, variations in mantle source composition (X), and the extent to which it melts (F, also called melt fraction). In principle, these can be constrained by experimental petrology and parameterization of its results [*Asimow et al*., 2001; *Longhi*, 2002; *Herzberg and O'Hara*, 2002; *Herzberg and Asimow*, 2008; *Kimura et al*., 2009]. However, a primary magma composition also depends on how the mantle melts, whether it is by batch, fractional, accumulated fractional, or some more complex melting process. Melts tend to drain from their sources by buoyant porous flow at low melt fractions [*Ahern and Turcotte*, 1979; *McKenzie*, 1984], so primary magmas are thought to form by the mixing of small melt droplets during decompression. This component can only be constrained computationally [*Langmuir et al*., 1992; *Herzberg and O'Hara*, 2002; *Herzberg and Asimow*, 2008] as its detailed simulation in the laboratory is not practical [*Asimow and Longhi*, 2004]. It is typically based on parameterizations of experimental data and is included as a fractional melting component in the forward model. It is important to consider because, at constant MgO and melt fraction, accumulated fractional melts can have substantially higher FeO contents than batch melts [*Herzberg and O'Hara*, 2002].

An inverse model attempts to reconstruct the processes of fractional crystallization in order to identify an array of potential melt or primary magma compositions that may have formed in the mantle. Unraveling the inverse process provides a partial solution to the primary magma problem, and many computational models are available [*Langmuir and Hanson*, 1980; *McKenzie and Bickle*, 1988; *Langmuir et al*., 1992;

Danyushevsky, 2001; *Herzberg and O'Hara*, 2002; *Herzberg and Asimow*, 2008; *Lee et al*., 2009; *Putirka et al*., 2007; *Kimura et al*., 2009]. The solution is only partial because multiply saturated lavas and even primitive olivine phyric lavas no longer contain complete information about their origin. At some stage, olivine must be added incrementally to move up in temperature toward more primitive compositions, and it is necessary to know at what point the computed melt reflects the primary magma composition in the mantle; that is, how do we know when to stop adding olivine?

In principle, an erupted basalt composition can have its primary magma composition constrained when there is commonality to the inverse and forward model components. The underlying theory was described by *Herzberg and O'Hara* [2002], and is described again in section 2 of this paper. The algorithm was first publicly implemented in software called PRIMELT1.XLS [*Herzberg et al*., 2007], and it is a mass balance solution to the primary magma problem for an assumed peridotite composition. PRIMELT is calibrated from experiments on peridotite KR4003 [*Walter*, 1998] and parameterizations of these and other experiments [*Herzberg and O'Hara*, 2002]. PRIMELT1.XLS [*Herzberg et al*., 2007] was limited to spinel peridotite and harzburgite melting; this was followed by PRIMELT2.XLS, which included garnet peridotite melting and additional tests for suitability of the method for the input sample composition [*Herzberg and Asimow*, 2008]. In this paper, we report PRIMELT3 MEGA.XLSM, which differs from its predecessors in the following ways.

1. Improvements were made to melt fractions in projection space.

2. The residuum mineralogy is identified.

3. Approximations to olivine liquidus temperatures at 1 atmosphere were replaced by more accurate temperatures.

4. Olivine liquidus temperatures in T-P space are used to provide new insights into mantle potential temperature and its uncertainties. This is made tractable by a computed peridotite solidus, a new feature.

5. PRIMELT2 computes the Ni contents of coexisting olivine and liquid using partition coefficients from *Beattie et al*. [1991], but a small error was reported to us by J.-I. Kimura (personal communication, 2011), and this was corrected in PRIMELT3.

6. MEGA refers to a macroenabled option that can batch process a list of input compositions automatically, which is very useful for large data sets.

We provide a brief review of the inverse and forward model components of all PRIMELT models using the improvements that have been made. However, the interested user is encouraged to read the many features of PRIMELT2 [*Herzberg and Asimow*, 2008] that we have carried unmodified to its present form. The more important of these are discussed in abbreviated form in the Appendix A. These are error codes that describe whether the primary magma composition has been adversely compromised by clinoproxene addition/subtraction, pyroxenite melting, or the effects of CO_2 on melting. We also provide in the Appendix A an abbreviated summary of all computational uncertainties.

A copy of PRIMELT3 MEGA.xlsm is provided in supporting information S1, and information about its content is given in the Appendix A. PRIMELT3 has been applied to lava compositions for which PRIMELT2 primary magma solutions were previously reported [*Herzberg et al*., 2007; *Herzberg and Asimow*, 2008; *Herzberg and Gazel*, 2009]. In general the differences between PRIMELT2 and PRIMELT3 primary magma solutions are small, and prior inferences regarding mantle potential temperature remain mostly unmodified. However, we will revisit a number of applications with the intention of providing a more rigorous estimation of uncertainties in olivine liquidus temperature, mantle potential temperature, and anhydrous peridotite solidus temperatures.

2. PRIMELT3 Melt Fractions

An example of how PRIMELT3 works to constrain primary magma composition is given in Figure 1. The black cross is lava composition 1187-8 from the Ontong Java Plateau [*Fitton and Godard*, 2004] (FeO/FeO_T = 0.9) projected from Diopside into the plane Olivine-Anorthite-Quartz (Figure 1a) and in FeO-MgO space (Figure 1b). This is a primitive whole rock lava composition that is plausibly related to the primary magma composition by subtraction of olivine only. The choice of a primitive lava composition is important

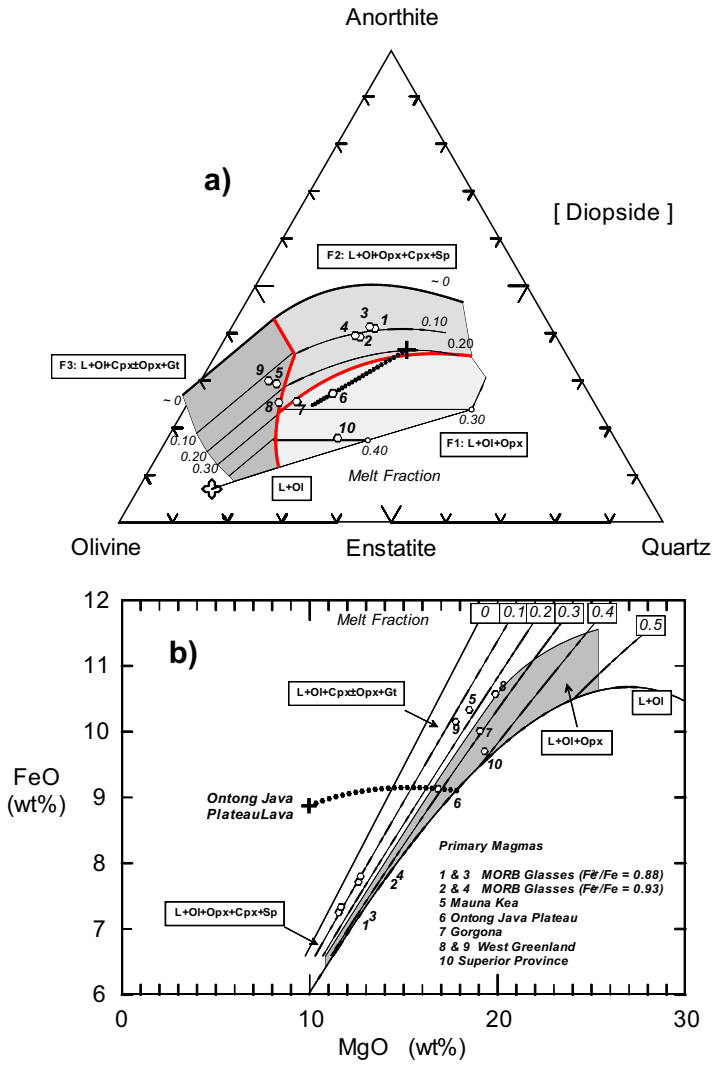

Figure 1. Illustration of primary magma calculation using forward models of peridotite melting in multicomponent and binary MgO-FeO projection spaces integrated with an inverse model of olivine addition. Arrays of black circles illustrate how a primary magma is computed from a lava composition, using a whole-rock composition from the Ontong Java Plateau (large black cross) as an example (see text); PRIMELT seeks a common melt fraction in both projections, providing a mass balance solution to the primary magma problem. Small open symbols with numbers are various primary magma solutions provided by PRIMELT3.xlsm (supporting information S1). (a) A multicomponent projection of liquid compositions (mole%) obtained by melting fertile mantle peridotite from Diopside into the plane Olivine-Anorthite-Silica [*Herzberg and O'Hara*, 2002]. All weight % compositions are converted to mole %, and projection coordinates are calculated in the following way:
Olivine = 1.5 TiO_2 + 0.5 Al_2O_3 + 0.5 Cr_2O_3 + 0.5 FeO + 0.5 MnO + 0.5 MgO − 0.5 CaO − 0.5 Na_2O + 3.0 K_2O + 0.5 NiO
Anorthite = 1.0 TiO_2 + 1.0 Al_2O_3 + 1.0 Cr_2O_3
Quartz = 1.0 SiO_2 − 0.5 Al_2O_3 − 0.5 Cr_2O_3 − 0.5 FeO − 0.5 MnO − 0.5 MgO − 1.5 CaO − 3.0 Na_2O − 3.0 K_2O − 0.5 NiO
Bold red lines separate three residuum lithologies. Black solid lines are melt fraction contours. Small hexagons labeled by numbers indicate successful primary magma solutions for a variety of lavas; see Figure 1b for legend. (b) A binary MgO-FeO projection of primary magma compositions formed by accumulated fractional melting, from *Herzberg and Asimow* [2008]. The symbols are the same as in Figure 1a.

because PRIMELT3 reconstructs the primary magma composition by addition or subtraction of olivine to the lava composition. PRIMELT3 cannot invert the liquid line of descent involving [L+Ol+Plag] or [L+Ol+Plag+Cpx].

Addition of olivine to the OJP lava composition produces an array of potential primary magma compositions in both Ol-An-Qz and FeO-MgO projection space. But how do we know when to stop adding olivine? Most petrological models stop adding olivine when the liquid composition is in equilibrium with an assumed olivine composition, typically having an Mg-number of 90 or 91. In contrast, the PRIMELT calculation is stopped when a common melt fraction is uniquely identified in both projection and FeO-MgO space,

which is 0.28 for the example considered in Figure 1. This is what is meant by a mass balance solution to the primary magma problem, given an assumed peridotite composition that was parameterized to yield melt fractions in Figure 1 (i.e., KR4003) [*Walter*, 1998; *Herzberg and O'Hara*, 2002]. PRIMELT3 computes olivine phenocrysts that would crystallize from the primary magmas, and these can have Mg-numbers ranging from 90 for relatively low-degree melts to 93 in very high-degree melts; the assumption of constant olivine composition can propagate to an error in mantle potential temperature of over 100°C. The primary magma for the Ontong Java Plateau has 16.85% MgO, the melt fraction was 0.28, the mantle potential temperature was 1483°C, and the predicted most primitive olivine phenocryst composition had an Mg-number of 91.5. These results can be found in the worksheet 'OJP' in PRIMELT3 MEGA.xlsm, given in supporting information S1.

Melt fractions in FeO-MgO space (Figure 1b) are identical to those reported in *Herzberg and Asimow* [2008] for PRIMELT2 and for the case of primary magmas produced by accumulated fractional melting. However, melt fractions shown in Ol-An-Qz are an improvement over those reported for PRIMELT2. This projection identifies melt fractions for residuum mineralogies that consist of spinel peridotite, garnet peridotite and harzburgite. Unlike FeO-MgO space, melt fractions in Ol-An-Qz display discontinuities where one residue changes to another, as revealed by the red lines in Figure 1a. The condition where there is a unique melt fraction for two residues is satisfied to good approximation along the red boundaries, but misfits were discovered for PRIMELT2 and these have been corrected.

Here we use three expressions that capture the behavior of melt fraction in Ol-An-Qz for three different residual lithologies (Figure 1a). For melt extraction from residues of harzburgite (the meaning of the residual mineralogy names we adopt is explained below):

$$F1 = 6.2819An^2 - 14.7789An^3 + 0.00825(1/An)^2 \quad (1)$$

PRIMELT3 adopts F1 from PRIMELT2 [*Herzberg and Asimow*, 2008] without modification.

For melt fraction from residues of spinel peridotite:

$$F2 = X + YOl + Z/Ol \quad (2)$$

where:

$$X = (X1 + X2)/2 \quad (3)$$

$$Y = Qz^{0.245}\exp(0.931 + 1.623Qz) \quad (4)$$

$$Z = Qz^{0.577}\exp(0.769 - 7.514Qz) \quad (5)$$

and:

$$X1 = -1.994 + 2.25Qz + 0.041/Qz \quad (6)$$

$$X2 = -1.183 - 3.005Qz + 13.774Qz^2 - 12.615Qz^3 \quad (7)$$

For melt fraction from residues of garnet peridotite:

$$F3 = -2.5345 + 5.329(Qz + 0.348Ol) + 0.3012/(Qz + 0.348Ol) \quad (8)$$

Ol, An, and Qz in equations (1)–(8) are coordinates for liquids that project from diopside into the plane olivine-anorthite-silica; their calculation is given in the caption to Figure 1.

PRIMELT3 melt fractions are similar to those of PRIMELT2 for garnet peridotite and harzburgite melting (Figure 2a). The most significant improvement is for elevated melt fractions appropriate to spinel peridotite melting. However, as discussed below, these differences in melt fractions do not propagate to large differences in inferred mantle potential temperature (Figure 2b).

3. Source Residuum Mineralogy and Composition

PRIMELT3 uses the Ol-An-Qz projected compositions of primary magmas to identify the residuum mineralogy from which it separated. It is important to note, however, that an aggregate fractional melt is not in equilibrium with its residue. Only the final drop of liquid extracted is in equilibrium with the residue.

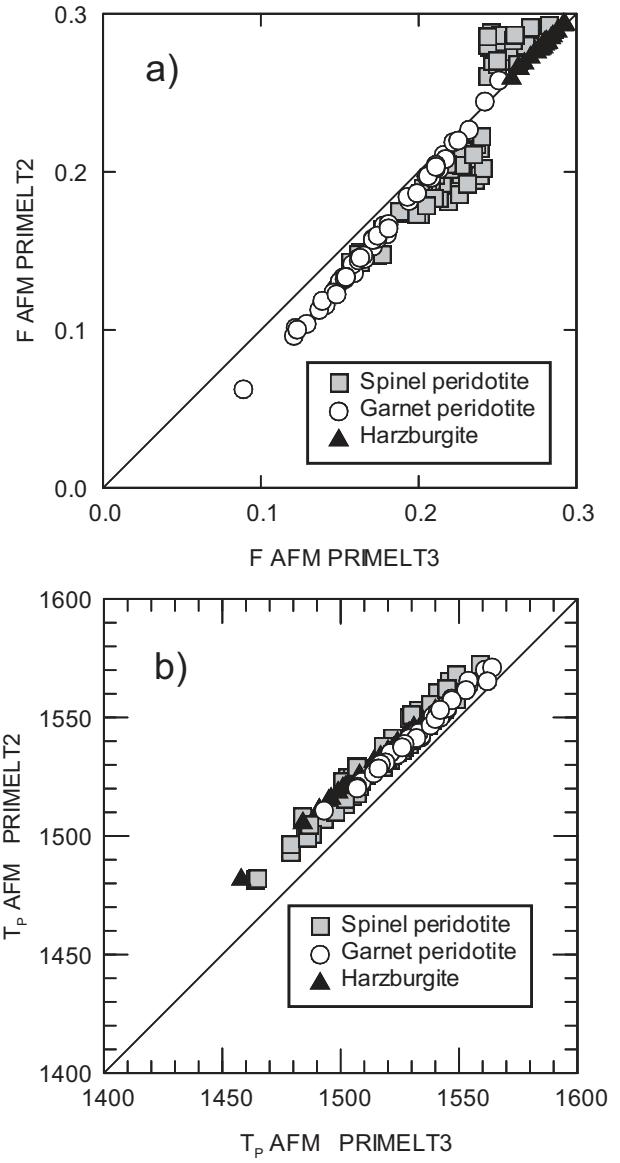

Figure 2. A comparison of inferred melt fractions for PRIMELT3 and PRIMELT2, using successful solutions to the primary magma problem for Paleocene picritic lavas from West Greenland [*Larsen and Pedersen*, 2009]. (a) The largest misfits arise from high melt fractions of spinel peridotite. (b) Melt fraction differences do not propagate to significant differences (i.e., $\leq$20°C errors) in inferences drawn about mantle potential temperature T_P.

Nevertheless, mass balance is maintained with an equation that is identical to that for batch melting [*Herzberg*, 2004]:

$$C_o = FC_L + (1-F)C_S \quad (9)$$

where C_o is the initial source composition, F the mass fraction of the aggregate melt, C_L is the aggregate liquid composition, and C_S is the composition of the residue in equilibrium with the last drop of liquid extracted. We therefore refer to the residues as the solid that was left behind, not the solid in equilibrium with the aggregate primary melt. Also, any complementary residue is only strictly valid for a melting situation that occurs along a single streamline for both liquid and solid, most appropriate for simple cylindrical melting regimes. This is not likely to be realized even for plumes which deform as they impact the base of a lithosphere. And it is clearly not true of an aggregate fractional melt extracted from corner-flow driven melting regimes below oceanic ridges, which leave behind many residues with variable extents of depletion. PRIMELT3 does not compute residuum composition, but the reader can easily do this using equation (9) and the composition of peridotite KR4003 [*Herzberg and O'Hara*, 2002, Table 1]; in view of the above mentioned complexities, a residue so computed may be considered a "mean" composition. Satisfactory residue compositions are obtained for the major elements SiO_2, Al_2O_3, FeO, MgO, and CaO, and these can be used to compute temperatures and pressures of melting [*Lee and Chin*, 2014]. However, compared with typical peridotites of similar fertility, KR4003 is somewhat deficient in TiO_2,and Na_2O, high in K_2O, and P_2O_5 has not been determined. Hence, residue compositions calculated for these minor elements will not be reliable.

We have used the general terms spinel peridotite and garnet peridotite for the clinopyroxene-bearing residual mineralogies rather than the more conventional term "lherzolite" because there are important variations and uncertainties in peridotite mineralogy that remain poorly constrained. The rock name lherzolite specifically requires the presence of modal olivine, orthopyroxene, and clinopyroxene; yet the presence of orthopyroxene at high pressure is composition dependent, poorly constrained and controversial. For example, the thermodynamic model of *Holland et al*. [2013] indicates garnet lherzolite melting (L+Ol+Opx+Cpx+Gt) of the composition KLB-1 transforms to garnet peridotite melting (L+Ol+Cpx+Gt) at $>$ 3.2 GPa, but the stability of orthopyroxene depends critically on peridotite composition. Also, spinel lherzolite transforms to lherzolite $\pm$ minor Cr spinel with increasing temperature and melt fraction. For example, the modal

abundance of spinel drops dramatically when F > 0.10 in melting experiments on peridotite MM3 at 1 GPa [*Baker and Stolper*, 1994]. Spinel in many naturally occurring harzburgites ranges from ~ 0 to 1.5% in the mode [*Doucet et al*., 2012]. Most likely, temperature will determine whether garnet lherzolite (or peridotite) transforms to spinel peridotite or harzburgite on decompression. Also, there is a stability field of garnet harzburgite [L+Ol+Opx+Gt] that separates [L+Ol+Cpx+Gt] from [L+Ol+Opx] [*Walter*, 1998; *Herzberg and O'Hara*, 2002], although it is restricted and, for simplicity, not represented in Figure 1a. In summary, the residues that are typically produced during decompression melting are:

garnet peridotite (Ol + Cpx + Gt ± Opx)

⇩

spinel peridotite (Ol + Opx + Cpx + spinel (Al or Cr))

⇩

harzburgite (Ol + Opx ± chrome spinel)

When a primary magma solution is constrained, it is necessary to compare melt fractions for accumulated fractional melting in MgO-FeO space (i.e., F_{AFM}) with melt fractions from the different possible residues as shown in Figure 1a (i.e., $F1_{Proj}$, $F2_{Proj}$, $F3_{Proj}$ in Figure 1a). PRIMELT3 uses the following procedure:

If $F_{AFM} = F1_{Proj}$, then the residuum = harzburgite.

If $F_{AFM} = F2_{Proj}$, then the residuum = spinel peridotite

If $F_{AFM} = F3_{Proj}$, then the residuum = garnet peridotite

The critical projected contour that bounds clinopyroxene stability in Ol-An-Qz plots at coordinates:

$$Qz_{CPX} = -0.074 + 0.1713/Ol - 0.0135/Ol^2 \quad (10)$$

such that harzburgite is the residuum if $Qz > Qz_{CPX}$.

Projection coordinates that separate residues of garnet peridotite from spinel peridotite or harzburgite are defined by:

$$Qz_{LZ/HZ} = (16.843 + 28.733An - 14.183\exp(An))^{-1} \quad (11)$$

such that garnet peridotite is the residuum if $Qz < Qz_{LZ/HZ}$ and also if Ol > 0.5.

4. Olivine Liquidus Temperatures

PRIMELT3 computes the composition of olivine in equilibrium with liquid in the inverse model. This requires knowledge of the Fe-Mg partitioning between these phases, also called K_D, and the method of *Toplis* [2005] was adopted. There is a temperature dependency to the calculation of K_D in the *Toplis* [2005] model and PRIMELT2 used a simplified version of the method of *Beattie* [1993] as given in *Herzberg and Asimow* [2008, equation (12)]. For primary magmas with MgO = 10–30%, representative of MORB basalts to komatiites, the average difference between the *Beattie* T and modified *Beattie* T is 8°C, well within the ±31°C (2σ) uncertainty stated by *Beattie* [1993]. However, this difference gets larger for liquids with MgO contents outside the 10–30% bounds. Therefore, PRIMELT3 has adopted the original olivine liquidus temperatures from *Beattie* [1993] for all calculations. These are given in cells O11 and O15 and column AE in the PRIMELT3 worksheets.

The olivine liquidus temperature is an important way of evaluating the thermal propoperties of primary magmas and their derivative melts, and many empirical petrological models have been used. Of these, *Beattie* [1993], *Ford et al*. [1983], *Sugawara* [2000], and *Ariskin et al*. [1993] reported the results of parameterizations of large numbers of experimental observations. These and other models were reviewed by *Putirka et al*. [2007], who concluded that the method of *Beattie* [1993] was the most accurate in predicting anhydrous experimental observations when pressure corrections from *Herzberg and O'Hara* [2002] were adopted. This is provided again:

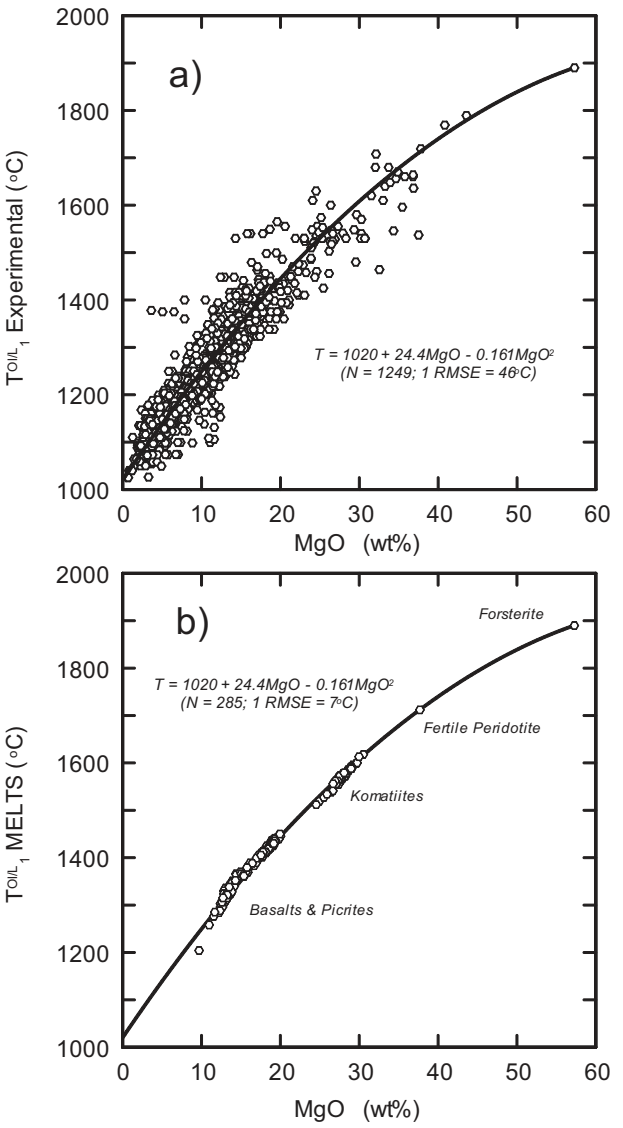

Figure 3. Olivine liquidus temperatures at 1 atmosphere. (a) An anhydrous experimental database and a model description. (b) A comparison of the experimental model $T_1^{Ol/L}$ with those derived from MELTS [*Ghiorso and Sack*, 1995] on a representative range of compositions.

$$T_P^{Ol/L}(°C) = T_1^{Ol/L} + 54P - 2P^2 \quad (12)$$

where $T_P^{Ol/L}$ is the olivine liquidus temperature in °C at pressure P in gigapascals, $T_1^{Ol/L}$ is the olivine liquidus temperature at 1 atmosphere (°C) [*Beattie*, 1993], and the pressure constants describe the effect of pressure on increasing olivine liquidus temperature [*Herzberg and O'Hara*, 2002; *Herzberg and Asimow*, 2008]. Application of the *Beattie* [1993] thermometer to 521 experimental glasses at 1 atmosphere and without water has a 1 σ uncertainty of $\pm$ 23.8°C [*Putirka et al*., 2007]. The pressure terms up to 7 GPa add an uncertainty of $\pm$ 31°C [*Herzberg and O'Hara*, 2002]. The total uncertainty in temperature at all pressures is $(23.8^2 + 31^2)^{0.5} = 39$°C ($\pm 1\ \sigma$), in good agreement with $\pm$ 38.5°C from 870 experiments reported by *Putirka et al*. [2007].

We are interested in mapping the MgO content of melts in T-P space between the anhydrous peridotite liquidus and solidus, as discussed in the section that follows. In order to simplify this calculation, we obtain the olivine liquidus temperature as a function of the weight% MgO content of the melt by parameterizing 1248 anhydrous experiments containing olivine and quench melt, conducted from 1025 to 2020°C and 1 atmosphere to 14 GPa; this is an upgrade of a database used by *Putirka et al*. [2007] and kindly supplied to us (K. Putirka, personal communication, 2014). The parameterization was pinned to the 1 atmosphere melting temperature of pure forsterite Mg_2SiO_4 (1890 $\pm$ 20°C) [*Bowen and Andersen*, 1914], which remains a point of reference for all subsequent high pressure experimental studies [*Davis and England*, 1964; *Ohtani and Kumazawa*, 1981; *Presnall and Walter*, 1993] and for olivine liquidus models [*Beattie*, 1993; *Ghiorso and Sack*, 1995]. All experimental temperatures conducted at pressures greater than 1 atmosphere were corrected to 1 atmosphere (i.e., $T_1^{Ol/L}$) using the pressure terms in equation (12), yielding:

$$T_1^{Ol/L} = 1020 + 24.4MgO - 0.161MgO^2 \quad (13)$$

where $T_1^{Ol/L}$ is in °C. Equation (13) captures experimental olivine liquidus temperatures with a 1σ root mean square error of $\pm$ 46°C (Figure 3a); this uncertainty is only marginally higher than $\pm$ 41°C using the *Beattie* [1993] thermometer for this expanded database, but it has the advantage of requiring only one variable melt compositional term to describe $T_1^{Ol/L}$ (i.e., MgO) rather than 8 terms. Equation (13) can be applied to a wide range of melt compositions: MgO = 1–57%; $Na_2O + K_2O$ = 0–14%; SiO_2 = 30–70%.

We compare our new thermometer with that based on MELTS [*Ghiorso*, 1994; *Ghiorso and Sack*, 1995], which differs in using experimental data to parameterize the temperature at which the Gibbs energy is

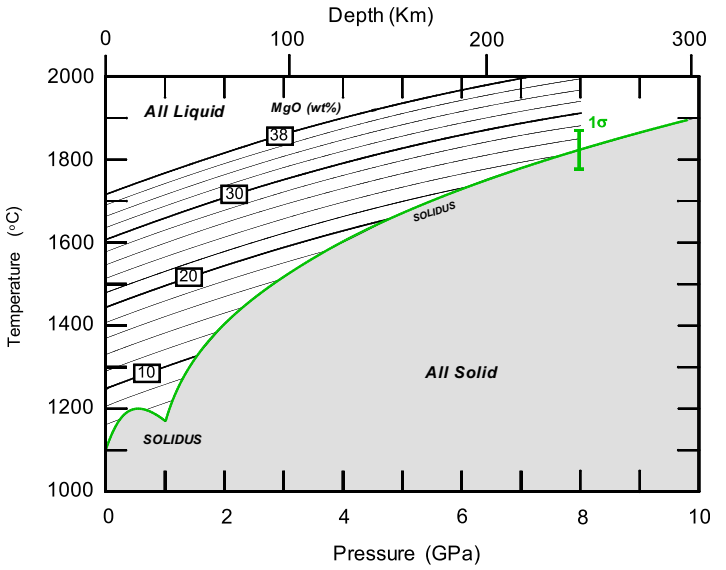

Figure 4. Olivine liquidus temperatures for partial melts of peridotite KR4003 as functions of MgO content and pressure, from equations (12) and (13) in the text. MgO contents of liquids on the solidus are given in the following Figure 5, providing unique T-P solutions to the peridotite solidus at pressures >1 GPa. The 1σ bracket represents T uncertainties from equation (13).

minimized for any olivine-liquid pair. We have applied MELTS to estimate the temperature at which olivine is in equilibrium with a wide range of melt compositions. These are new PRIMELT3 primary magma solutions to lava compositions for which PRIMELT2 primary magma solutions were reported [*Herzberg et al*., 2007; *Herzberg and Asimow*, 2008; *Herzberg and Gazel*, 2009], in addition to primary magmas for Archean komatiites [*Herzberg et al*., 2010; see Appendix] and peridotite KR4003 [*Herzberg and O'Hara*, 2002]. Our empirical thermometer described by equation (13) can reproduce MELTS temperatures to within $\pm$ 7°C (Figure 3b).

5. MgO Contents of Primary Magmas and the Anhydrous Peridotite Solidus Revisited

In regions removed from subduction zones, major melting of peridotite begins when the mantle rises buoyantly to the anhydrous solidus, and further melting progresses as the temperature drops during continued adiabatic decompression. Forward simulations of peridotite partial melting during adiabatic decompression require knowledge of solidus temperatures, the heat of fusion, heat capacity, and thermal expansivity. Many such simulations have been published, and the T-P paths differ because of differing assumptions about the thermodynamic terms and how they change throughout the melting interval [*Cawthorn*, 1975; *McKenzie and Bickle*, 1988; *Langmuir et al*., 1992; *Iwamori et al*., 1995; *Asimow et al*., 2001; *Putirka et al*., 2007]. What we seek is a petrological model that describes how primary magma compositions vary during a T-P decompression journey. More specifically, we examine how their MgO contents change, and how well they are described by forward simulations that differ in their assumed thermodynamic properties.

Figure 4 is a map of the MgO contents of liquids in equilibrium with olivine for peridotite KR4003 [*Herzberg and O'Hara*, 2002], obtained by analytical solutions to the equations (12) and (13). For convenience, it was solved for equilibrium melting of peridotite KR4003, but solutions are perfectly general and valid for fractional melting and for all residuum lithologies. Equations (12) and (13) provide an opportunity to compute the T-P conditions of the anhydrous peridotite solidus if the MgO content along it can be independently constrained and with the condition that $P = P_{solidus}$. We obtained a fit to this relation for $P \geq 1$ GPa:

$$P_{solidus} = MgO^{-0.52} \exp(0.13 + 0.15MgO) \quad (14)$$

The following are experimental sources that were used for this calibration: 1.0 GPa [*Baker and Stolper*, 1994; extrapolated to F = 0]; 3 GPa [*Davis et al*., 2011]; 5.0 and 9.7 GPa [*Herzberg and Zhang*, 1996]; 6 and 7 GPa [*Walter*, 1998] (data on L+Ol+Cpx$\pm$Opx+Gt extrapolated to zero from F in the 0.11–0.41 range). It is important to note that *Walter*'s data at 6 and 7 GPa yield linear arrays in MgO-FeO space over a wide range of F, and these arrays accurately intersect the array of MgO-FeO contents of liquids on the solidus (see discussion in *Herzberg and O'Hara* [2002]). The MgO contents of melts on the anhydrous peridotite solidus are shown in Figure 5, and equation (14) reproduces all experiments in the 1–9.7 GPa range to within $\pm$ 0.3 GPa in most cases. Our parameterization indicates there are large changes in the MgO contents of near-solidus

melts in the 1.0–1.5 GPa range, and it is broadly in agreement with other studies [*Robinson et al*., 1998; *Falloon et al*., 2008; *Chalot-Prat et al*., 2010, 2013].

The new solidus shown in Figure 4 can be described by the equation:

$$T_{solidus} = \exp\left(7.12 - 0.06/(P_{solidus})^4 + 0.187 * \ln(P_{solidus})\right) \quad (15)$$

where $T_{solidus}$ is the solidus temperature at pressure $P_{solidus}$ in the 1.0–7.0 GPa range. This is the range for which the pressure terms in equation (12) were derived [*Herzberg and O'Hara*, 2002], and the 1σ uncertainty in temperature is $\pm$ 46°C. It is not clear whether equation (15) is valid at pressures beyond 7 GPa; however, it also satisfies the T-P conditions of the anhydrous solidus at 15.3 GPa, the olivine-wadsleyite transition [*Herzberg and Zhang*, 1996; *Herzberg et al*., 2000].

We now evaluate how our computed peridotite solidus compares with experimental observations, and results are shown in Figure 6. *Hirschmann* [2000] and *Herzberg et al*. [2000] showed that solidus temperatures are lowered with elevated alkalis and lower Mg-numbers, and this has been confirmed [*Laporte et al*., 2014]. We therefore restrict this analysis to experimental data on peridotites KLB-1 and KR4003, which are only moderately depleted in MgO with respect to the *McDonough and Sun* [1995] pyrolitic mantle. It is notable that *Walter* [1998] reported a whole rock composition for KR4003 with 37.3% MgO, but the total is low (i.e., 99.18%) and the Mg-number for this composition is 89.2, in contrast with 89.5 for olivine in subsolidus experiment 60.02. As discussed in *Herzberg and O'Hara* [2002], an MgO content of 38.12% for KR-4003 brings the total to 100%, raises its Mg-number to 89.4, and predicts 89.4–89.5 for solidus olivine. Data sources for the solidus brackets shown in Figure 5 are: *Canil* [1992], *Takahashi* [1986], *Takahashi et al*. [1993], *Hirose and Kushiro* [1993], *Herzberg et al*. [2000], *Walter* [1998], *Lesher et al*. [2003], and *Davis et al*. [2011]. Our computed anhydrous solidus and its temperature uncertainty are consistent with this experimental database and previous parameterizations [*Herzberg et al*., 2000; *Hirschmann*, 2000]. However, temperatures at 2 GPa are higher, and temperatures in the 7–10 GPa range are lower, the latter being more consistent with the experimental observations of *Walter* [1998] and *Herzberg et al*. [2000].

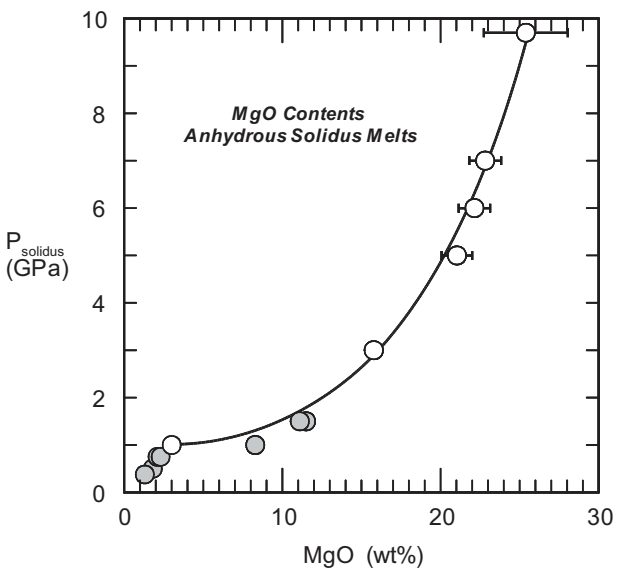

Figure 5. Pressures of initial melting on the anhydrous peridotite solidus and the MgO content of the near-solidus melts of mantle peridotite. Open circles used in the parameterization are experimentally constrained melt compositions from *Baker and Stolper* [1994], *Davis et al*. [2011], *Herzberg and Zhang* [1996], and *Walter* [1998]. Closed circles (not used in the parameterization for pressures $\geq$1 GPa) are near-solidus melt compositions from *Robinson et al*. [1998], *Falloon et al*. [2008], and *Chalot-Prat et al*. [2010, 2013]. Error bars for *Herzberg and Zhang* [1996] are 1σ uncertainty arising from electron microprobe analysis. Error bars for *Walter* [1998] are 1σ uncertainty arising from uncertainty in Fe-Mg partitioning between olivine and melt [*Herzberg and O'Hara*, 2002].

6. MgO Contents of Primary Magmas and Mantle Potential Temperature

We are now positioned to evaluate uncertainties in estimating mantle potential temperature T_P from the MgO content of a PRIMELT3 primary magma. Shown in Figure 7 are the MgO contents of partial melts and solid-state adiabatic gradients from *Iwamori et al*. [1995]. It is notable that the Iwamori et al. adiabatic temperature profile having a T_P of 1300°C is nearly identical to the most recent determination of *Katsura et al*. [2010] based on new thermoelastic parameters of olivine. While there are significant differences in forward models of adiabatic gradients in the melting region, the ones given by *McKenzie and Bickle* [1988], *Langmuir et al*. [1992], *Iwamori et al*. [1995], *Asimow et al*. [2001], and *Putirka et al*. [2007] are

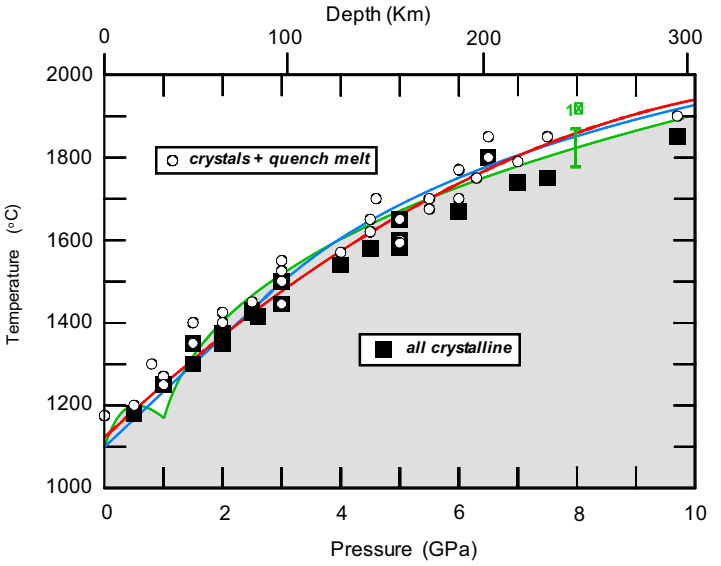

Figure 6. The new computed anhydrous peridotite solidus (green curve) and experimental constraints (open circles and closed squares). The 1σ bracket represents T uncertainties from equation (13) in the text. Red and blue curves are solidus curves from *Hirschmann* [2000] and *Herzberg et al*. [2000], respectively.

coincident with the isopleths of MgO in Figure 7 to within ± 1.5 weight%. For preservation of clarity, we illustrate this coincidence with adiabatic melting paths obtained from MELTS and pMELTS (Figure 7a). These curves are generally similar in shape, reflecting the increase in melt productivity from the solidus up to the exhaustion of clinopyroxene in both models. Although pMELTS predicts a somewhat higher overall melt productivity and hence a steeper thermal gradient in the melting region, both models predict gradients that approximately parallel the MgO isopleths. The observation of coincidence was originally made by *Herzberg and O'Hara* [2002], and it provided the basis for calibrating T_P from the MgO content of a primary magma [*Herzberg et al*., 2007; *Herzberg and Asimow*, 2008, equation (13)]. The present work is a confirmation of the earlier study, but here it provides the basis for an updated calibration and uncertainty analysis.

The intersections of the solid-state adiabatic gradients with the anhydrous peridotite solidus having the weight% melt MgO contents shown in Figure 7 yields:

$$T_P = 1025 + 28.6\mathrm{MgO} - 0.084\mathrm{MgO}^2 \quad (16)$$

where T_P is the mantle potential temperature in °C. Any thermodynamic adiabatic gradient model in the melting region that differs from the MgO isopleths shown in Figure 7 by ± 1.5 weight % will propagate to an uncertainty in T_P of < ± 42°C. As existing adiabatic melting models satisfy this condition, mantle potential temperatures computed from equation (16) with PRIMELT3 primary magma MgO contents should be accurate to within ± 42°C.

Application of equation (16) to PRIMELT3 primary magma MgO contents yields mantle potential temperatures that are similar to those of PRIMELT2 [*Herzberg and Asimow*, 2008], except that they are lower by ~ 17°C on average. PRIMELT3.xlsm provides new T_P estimates from equation (16) in cell Q15; the potential temperature calculation from PRIMELT2 is also shown in cell P15 for comparison. Results for MORB and representative lava compositions from various OIB, LIP, and Archean komatiites are summarized in Figure 7b. Each OIB and LIP occurrence has primary magma MgO contents that exhibit a 2–4% MgO range, equivalent to a T_P range of ~50–100°C. This has been interpreted to reflect temperatures that are hotter in the axis of the plume relative to the periphery [*Herzberg and Asimow*, 2008; *Herzberg and Gazel*, 2009]. OIB and LIPS are focussed sources of heat and magmatism, not the products of broad upwellings [*Anderson and Natland*, 2014]. Therefore, maximum MgO contents should be most diagnostic of each mantle plume, and only these are provided in Figure 7b together with their inferred T_P maxima. PRIMELT3 predicts T_P increases in the following order: Siqueiros MORB < Galapagos = Canary Islands < Iceland < Gorgona komatiites < Mauna Kea (postshield, Hawaii) < Archean komatiites.

Olivine liquidus temperatures at 1 atmosphere for Gorgona komatiites and Siqueiros MORB (Figure 7b) are in good agreement with temperatures inferred from the aluminum content of olivine in equilibrium with spinel [*Coogan et al*., 2014]. Collectively, these results support the mantle plume model for LIP and OIB occurrences. PRIMELT3 cannot in general provide primary magma compositions for Archean komatiites (see

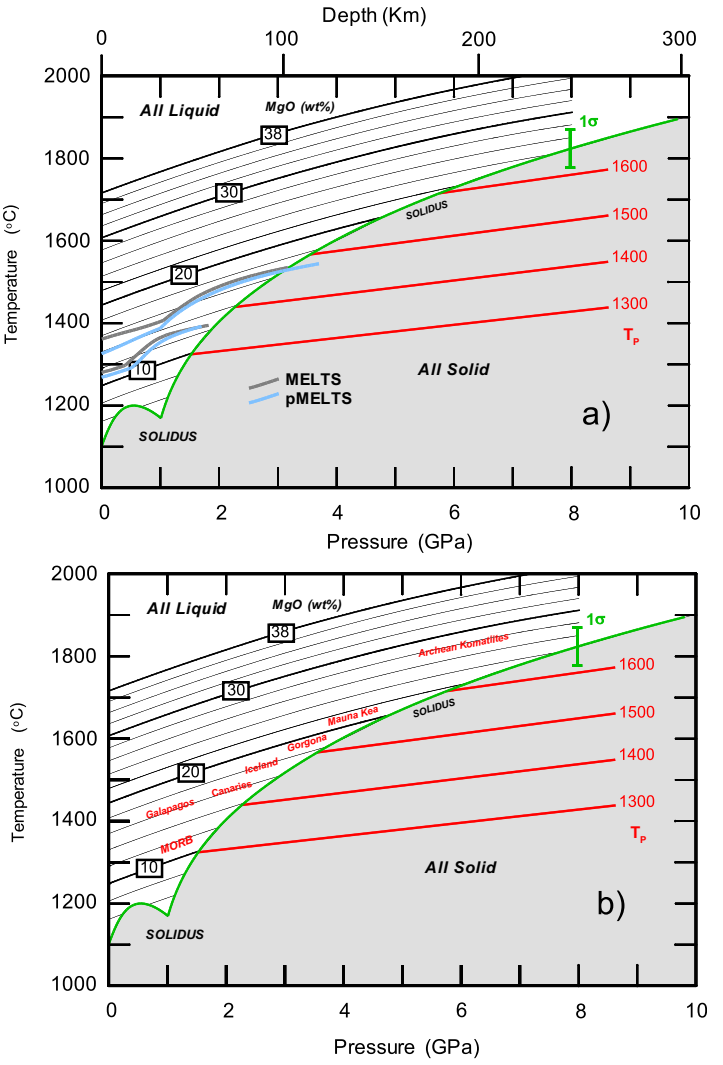

Figure 7. MgO contents of partial melts of mantle peridotite and mantle potential temperatures. (a) Gray and blue curves are example adiabatic gradients in the supersolidus region from MELTS [*Ghiorso*, 1994; *Ghiorso and Sack*, 1995] and pMELTS [*Ghiorso et al*., 2002]. (b) Maximum MgO contents of PRIMELT3 primary magmas for Siqueiros MORB and selected ocean islands, large igneous provinces, and Archean komatiites, and their inferred T_P (see worksheets for PRIMELT3 MEGA.XLSM).

Appendix A), but olivine phenocrysts and whole rock analyses constrain MgO to 26–30% [e.g., *Puchtel et al*., 2004; *Arndt et al*., 2008; *Herzberg*, 2011; *Herzberg et al*., 2010]. Extremely deep melting and T_P in excess of 1700°C are inferred for Archean komatiites (Figure 7b).

High MgO primary magmas formed in a hot mantle with elevated T_P must also crystallize olivine at high liquidus temperatures should they erupt at the surface. Mantle potential temperature T_P is related to olivine liquidus temperature at 1 atmosphere $T_1^{Ol/L}$ by the equation:

$$T_P = 1.049T_1^{Ol/L} - 0.00019\left(T_1^{Ol/L}\right)^2 + 1.487\cdot 10^{-7}\left(T_1^{Ol/L}\right)^3 \quad (17)$$

where both temperature terms are in °C.

7. Nickel Contents of Peridotite-Source Primary Magmas

Lavas that originate by the mixing of primary magmas with olivine-fractionated derivative liquids can have elevated Ni contents [*Herzberg et al*., 2014]; mixing can occur anywhere, such as during magma chamber recharge or in lava flows. Application of PRIMELT3 to such lavas will yield primary magmas that are too high in NiO because it cannot invert the mixing process. We recommend that the user instead compute the Ni content of the primary magma with the equation [*Herzberg*, 2011]:

$$\mathrm{Ni\ (ppm)} = 21.6\,\mathrm{MgO} - 0.32\,\mathrm{MgO}^2 + 0.051\,\mathrm{MgO}^3 \quad (18)$$

where MgO refers to the PRIMELT3 primary magma MgO content.

8. Conclusions

An upgrade of the PRIMELT algorithm [*Herzberg and O'Hara*, 2002] for calculating primary magma composition is given together with its implementation in PRIMELT3 MEGA.xlsm software. It is a mass balance solution to the primary magma problem for an assumed peridotite source, and it supersedes PRIMELT2.xls [*Herzberg and Asimow*, 2008]. The major improvements are that it corrects for mistakes in melt fraction and computed Ni content of olivine, it identifies residuum mineralogy, it provides a thorough analysis of uncertainties in mantle potential temperature and olivine liquidus temperature, and it

includes a batch-processing macro for handling large data sets automatically. The uncertainty analysis was made tractable by the computation of olivine liquidus temperatures as functions of pressure and partial melt MgO content, and it includes a new means of computing the anhydrous peridotite solidus in T-P space. A successful PRIMELT3 primary magma solution for a basalt provides the user the following information: primary magma composition, melt fraction (F), mantle potential temperature T_P, olivine liquidus temperatures at 1 atmosphere, olivine phenocryst composition at the liquidus, residuum mineralogy, and (with some caveats) residuum composition. Results of the application of PRIMELT3 to a wide range of basalts shows that the mantle sources of ocean islands and large igneous provinces were hotter than oceanic spreading centers, consistent with earlier studies and predictions of the mantle plume model.

Appendix A

As described in the text, PRIMELT3 MEGA.xlsm has a number of capabilities that were built into its predecessor PRIMELT2.xls, and readers are encouraged to read *Herzberg and Asimow* [2008] for a comprehensive description of its many features, including uncertainties. We begin by highlighting a few of the new operational details, and discuss how they impact earlier discussions about uncertainties.

A1. Using PRIMELT3 MEGA.xlsm for Primary Magma Calculation

We have provided in 7 separate worksheets example primary magma calculations for lavas from Mauna Kea [*Stolper et al*., 2004], Ontong Java Plateau [*Fitton and Godard*, 2004], Gorgona [*Arndt et al*., 1997], West Greenland [*Larsen and Pedersen*, 2009], Iceland [*Sinton et al*., 2005], the Superior Province in Canada [*Fan and Kerrich*, 1997]. Additionally, new glass analyses were obtained for Siqueiros MORB from the East Pacific Rise. Sample numbers are given so that the interested reader may go to the original references where the lava analyses were reported and reproduce our calculations.

A new primary magma composition can be obtained by simply selecting one of the 7 worksheets (or, better, making a copy of one of these worksheets and assigning it a new name) and replacing the weight% oxides in row 4 with the new analysis of choice. Attention should be given the pressure of fractionation in bars at cell R6 (which affects olivine-liquid K_D) and to the Fe^{2+}/Fe_T setting at cell F5. If the user wishes to obtain Fe^{2+}/Fe_T by instead constraining Fe_2O_3/TiO_2 (see *Herzberg and Asimow*, 2008], enter this value in cell L5 and then click the button labeled "Calculate Fe^{2+}/Fe^*." Primary magma compositions and conditions of melting are given in row 11 for batch melting and row 15 for accumulated fractional melting. All discussions about primary magmas in this paper refer to the case of accumulated fractional melting. A new feature of PRIMELT3 MEGA.xlsm is that it allows the user to obtain primary magma information on large batches of measured compositions using the worksheet entitled MEGAPRIMELT3. To use this function, put sample names in column A and data in columns B through P (again, the option to fix Fe_2O_3/TiO_2 is available using column Q). Select the sample names (cells of column A) to be processed and then click the big button. Output will appear in columns R through BR: first warning flags, then batch melting output, then accumulated fractional melting output. You may switch to other applications while Excel is running the MEGA macro in the background.

A2. Using PRIMELT3.xlsm as a Calculator for Olivine Liquid Line of Descent

Like previous versions, PRIMELT3 MEGA.xlsm will add and subtract olivine to and from the input lava composition. It provides the Mg-number of olivine that would crystallize from the computed primary magma at the surface in cell S15. But a new feature is that it also provides the equilibrium olivine composition at each incremental step: down-temperature fractionation appears in rows 28–52, and up-temperature back-fractionation appears in rows 55–115, with liquid compositions in columns B through N and olivine compositions in columns P through AB. This can be used as a calculator for olivine liquid line of descent, and it can be applied to any basalt. For example, it can be applied to basalt that originated from a pyroxenite source; in this example, the reader will be warned of a pyroxenite error code, and information about temperatures, pressure, and melt fraction will not be valid.

PRIMELT3 computes the composition of olivine in equilibrium with liquid using Ni partition coefficients from *Beattie et al*. [1991], and Ti, Al, Cr, Ca and Mn partition coefficients from *Herzberg and O'Hara* [2002].

Olivine is assumed to contain no Fe^{3+}, Na, K, and P. The model of *Toplis* [2005] is used for the Fe-Mg exchange (i.e., K_D), which is computed from the input lava composition and olivine liquidus temperature [*Beattie*, 1993].

A3. Bulk Peridotite FeO and MgO Content

Cells R3 and R4 contain the bulk composition of peridotite KR-4003 for which PRIMELT has been calibrated. These are used for melt fraction calculation, which depends on bulk peridotite FeO and MgO [*Herzberg and O'Hara*, 2002; *Herzberg and Asimow*, 2008]. Varying these numbers is useful in reproducing experimental melt fractions from FeO-rich and poor peridotite [*Herzberg and O'Hara*, 2002]. However, in general, we encourage users to make no change here because their effects on primary magma composition and melt fraction have not been fully evaluated.

A4. Application to Archean Komatiites

PRIMELT3 cannot be used to solve the primary magma problem for any melt whose source reached such a high degree of melting that it exhausted all pyroxenes and left behind a residue of dunite, a problem that is mainly restricted to aluminum-undepleted komatiites [*Herzberg*, 2004]. PRIMELT requires in its forward model a range of MgO and FeO contents for any specific melt fraction, and this excludes melts extracted from a dunite residue (Figure 1b). Aluminum-depleted komatiites likely left behind residues of Ol+Cpx+Gt [*Herzberg*, 1992, 2004], but CaO is highly mobile during alteration and this will typically result in a composition that gets flagged as a pyroxenite source in a PRIMELT3 error code.

A5. Application to Fractionated Basalts

An enduring limitation of PRIMELT3 and its predecessors is that it can only reconstruct a primary magma composition for a lava that has gained or lost olivine as a sole phenocryst phase. For example, most MORB glasses and whole rocks differ from those from the Siqueiros Fracture Zone in that they have experienced variable amounts of plagioclase and clinopyroxene fractionation [e.g., *O'Hara*, 1968]; the crystallization sequence common to MORB is L+Ol, L+Ol+Plag, L+Ol+Plag+Cpx. Any attempt to restore primary magma composition by addition of olivine to a lava that in fact experienced olivine + plagioclase crystallization will produce the erroneous result of a hot source [*Herzberg et al*., 2007; *Till et al*., 2012]. There are graphical solutions to up temperature back-tracking L+Ol+Plag [*Herzberg et al*., 2007; *Till et al*., 2012] and it is possible to encode it in software [*Danyushevsky*, 2001]. There are also nonunique iterative search methods that can provide a candidate primary liquid that evolves to a given multiply saturated liquid composition (incorporated in the latest versions of alphaMELTS [*Smith and Asimow*, 2005] and PRIMACALC2 [*Kimura and Ariskin*, 2014]). However, small uncertainties in an improper inversion can result in large uncertainties in primary magma composition and inferred conditions of melting.

A6. Effects of H_2O and CO_2

It is commonly assumed that estimates of mantle potential temperature based on anhydrous parameterizations will be too hot if volatiles played a role. It is certainly true that volatiles can suppress solidus and liquidus temperatures, and cold mantle can melt at conditions below the anhydrous peridotite solidus. However, it is faulty logic to assume that a hot mantle source undergoing melting is necessarily cooled down in some way by volatiles. The major effect of volatiles on MORB, OIB, and LIP melting will be to increase melt productivity [e.g., *Asimow and Langmuir*, 2003].

A7. The Effects of Variable Peridotite Fertility

The effects of variable peridotite fertility on T_P are minor as discussed previously [*Herzberg and O'Hara*, 2002; *Herzberg and Asimow*, 2008]. Depleted peridotites yield much less magma than fertile peridotite, but there is little change in computed primary magma MgO and inferred T_P.

A8. Uncertainties

There are many sources of uncertainty in PRIMELT calculation of primary magma composition, and these have been discussed in *Herzberg and O'Hara* [2002] and *Herzberg and Asimow* [2008]. While PRIMELT3 MEGA.xlsm has not added to the uncertainties, it is important to provide an abbreviated review. These are:

1. Uncertainty in use of the *Beattie* [1993] olivine liquidus temperature calculation at 1 atmosphere is $\pm$ 31°C (1σ; see discussion in section 4) [*Putirka et al*., 2007].

2. A 1σ uncertainty in the K_D for Fe-Mg partitioning between olivine and liquid will contribute to $\pm$ 1% MgO [1σ; *Herzberg and O'Hara*, 2002], which propagates to $\pm$ 20°C in olivine liquidus temperature $T_1^{Ol/L}$ at 1 atmosphere, and to uncertainty in melt fraction of $\pm$ 0.05 [*Herzberg and O'Hara*, 2002].

3. An uncertainty in $Fe^{2+}/\Sigma Fe$ of 0.90$\pm$0.05 will propagate to $\pm$ 1% MgO ($\pm$ 20°C $T_1^{Ol/L}$). For MORB we use $Fe^{2+}/\Sigma Fe$ of 0.88 [*Bézos and Humler*, 2005], but new analytical results have suggested more oxidized conditions for MORB than previous estimates [*Cottrell and Kelley*, 2011]. Evidence for oxidized conditions for some ocean islands basalts was discussed previously [*Herzberg and Asimow*, 2008], and this can be accommodated by adjusting Fe_2O_3/TiO_2 in cell L5.

4. Uncertainties in thermodynamic decompression models propagate to an uncertainty in mantle potential temperature of $< \pm$ 42°C (see section 6).

5. Melt fraction uncertainties in multicomponent projection space (Figure 1a) do not contribute significantly to primary magma MgO content [*Herzberg and Asimow*, 2008]. This computational method is forgiving because melt fractions in MgO-FeO space are more highly restricted, and large variations in F are inferred from small increments of olivine addition and MgO (Figure 1b).

6. Clinopyroxene fractionation is common in intraplate magmatism, and has the effect of driving up the FeO content of the derivative melt [*Herzberg and Asimow*, 2008]. PRIMELT3 will calculate anyway the primary magma composition and mantle potential temperature, but the result is erroneous. Clinopyroxene addition and subtraction will perturb the CaO content of the melt, and PRIMELT provides filters for its detection in cell M13. CaO is also easily mobilized during greenschist facies metamorphism, and it may compromise primary magma calculation from metamorphosed samples in the same sense as clinopyroxene addition and subtraction [*Herzberg et al*., 2010].

7. Melts of carbonated peridotite can have MgO contents that are higher than noncarbonated peridotite [*Dasgupta et al*., 2007] and PRIMELT3 warns the user of this possibility as an error code in cell G7.

8. Primary magmas of some pyroxenite sources can have lower CaO contents compared with those of peridotite sources [*Herzberg*, 2006], although there may be important exceptions [*Herzberg*, 2011]. PRIMELT3 identifies pyroxenite sources as an error code in cell G7 for the case where the primary magma is too low in CaO to have originated from a peridotite source.

10. Instantaneous fractional melts do not always mix to produce an accumulated fractional melt [*Herzberg et al*., 2007; *Herzberg and Asimow*, 2008]. These often have unusually low contents of FeO, and they plot in a forbidden region below the curve labeled L+Ol in Figure 1b. The calculation will proceed anyway, but the user is alerted with the warning "FeO/MgO forbidden" in cell Q13.

Acknowledgments
We are grateful to Mike Perfit for providing samples from the Siqueiros Fracture Zone and to Chris Vidito for electron microprobe analyses of the glasses. Paula Antoshechkina is acknowledged for helping with MELTS olivine liquidus temperatures. Keith Putirka is thanked for helping with an uncertainty analysis and for providing his database of experimental compositions. Jun-Ichi Kimura is thanked for pointing out an error in PRIMELT2 and for a critical review of this paper. Cin-Ty Lee is thanked for a critical reading and editorial handling of this paper. Data sources used to calculate primary magmas are given in Appendix A. PDA acknowledges NSF grant GI-1226270. Mike O'Hara contributed to the thinking behind the PRIMELT model, and passed away during the submission of this paper.

References

Ahern, J. L., and D. Turcotte (1979), Magma migration beneath an ocean ridge, *Earth Planet. Sci. Lett.*, *46*,115–122.
Anderson, D. L., and J. H. Natland (2014), Mantle updrafts and mechanisms of oceanic volcanism, *Proc. Natl. Acad. Sci. U. S. A.*, *111*, E4298–E4304.
Ariskin, A. A., M. Y. Frenkel, G. S. Barmina, and R. I. Nielsen (1993), COMAGMAT: A FORTRAN program to model magma differentiation processes, *Comput. Geosci.*, *19*, 1117–1155.
Arndt, N. T., A. C. Kerr, and J. Tarney (1997), Dynamic melting in plume heads: The formation of Gorgona komatiites and basalts, *Earth Planet. Sci. Lett.*, *146*, 289–301.
Arndt, N. T., C. M. Lesher, and S. J. Barnes (2008), *Komatiite*, 467 pp., Cambridge Univ. Press, Cambridge, U. K.
Asimow, P. D., and C. H. Langmuir (2003), The importance of water to oceanic mantle melting regimes, *Nature*, *421*, 815–820.
Asimow, P. D., and J. Longhi (2004), The significance of multiple saturation points in the context of polybaric near-fractional melting, *J. Petrol.*, *45*, 2349–2367.
Asimow, P. D., M. M. Hirschmann and E. M. Stolper (2001), Calculation of peridotite partial melting from thermodynamic models of minerals and melts, IV. Adiabatic decompression and the composition and mean properties of md-ocean ridge basalts, *J. Petrol.*, *42*, 963–998.
Baker, M. B., and E. M. Stolper (1994), Determining the composition of high-pressure mantle melts using diamond aggregates, *Geochim. Cosmochim. Acta*, *58*, 2811–2827.
Beattie, P. (1993), Olivine-melt and orthopyroxene-melt equilibria, *Contrib. Mineral. Petrol.*, *115*, 103–111.
Beattie, P., C. Ford, and D. Russell (1991), Partition coefficients for olivine-melt and orthopyroxene-melt systems, *Contrib. Mineral. Petrol.*, *109*, 212–224.
Bézos, A., and E. Humler (2005), The $Fe^{3+}/\Sigma Fe$ ratios of MORB glasses and their implications for mantle melting, *Geochim. Cosmochim. Acta*, *69*, 711–725.
Bowen, N. L., and O. Andersen (1914), The binary system MgO-SiO_2, *Am. J. Sci.*, *37*, 4887–500.
Canil, D. (1992), Orthopyroxene stability along the peridotite solidus and the origin of cratonic lithosphere beneath Southern Africa, *Earth Planet. Sci. Lett.*, *111*, 83–95.

Cawthorn, R. G. (1975), Degrees of melting in mantle diapers and the origin of ultrabasic liquids, *Earth Planet. Sci. Lett.*, *27*, 113–120.
Chalot-Prat, R., T. J. Falloon, D. H. Green, and W. O. Hibberson (2010), An experimental study of liquid compositions in equilibrium with plagioclase + spinel lherzolite at low pressures (0.75 GPa), *J. Petrol.*, *51*, 2349–2376.
Chalot-Prat, R., T. J. Falloon, D. H. Green, and W. O. Hibberson (2013), Melting of plagioclase + spinel lherzolite at low pressures (0.5 GPa): An experimental approach to the evolution of basaltic melt during mantle refertilization at shallow depths, *Lithos*, *172-173*, 61–80.
Coogan, L. A., A. D. Saunders, and R. N. Wilson (2014), Aluminum-in-olivine thermometry of primitive basalts: Evidence of an anomalously hot mantle source for large igneous provinces, *Chem. Geol.*, *368*, 1–10.
Cottrell, E., and K. A. Kelley (2011), The oxidation state of Fe in MORB glasses and the oxygen fugacity of the upper mantle, *Earth Planet. Sci. Lett.*, *305*, 270–282.
Danyushevsky, L. V. (2001), The effect of small amounts of H_2O on crystallisation of mid-ocean ridge and backarc basin magmas, *J. Volcanol. Geotherm. Res.*, *110*, 265–280.
Dasgupta, R., M. M. Hirschmann and N. D. Smith (2007), Partial melting experiments on peridotite+CO_2 at 3 GPa and genesis of alkalic ocean island basalts, *J. Petrol.*, *48*, 2093–2124.
Davis, B. T. C., and J. L. England (1964), The melting of forsterite up to 50 kilobars, *J. Geophys. Res.*, *69*, 487–500.
Davis, F. A., M. M. Hirschmann and M. Humayun (2011), The composition of the incipient partial melt of garnet peridotite at 3 GPa and the origin of OIB, *Earth Planet. Sci. Lett.*, *308*, 380–390.
Doucet, L. S., D. A., Ionov, A. V. Golovin, and N. P. Pokhilenko (2012), Depth, degrees and tectonic settings of mantle melting during craton formation: Inferences from major and trace element compositions of spinel harzburgite xenoliths from the Udachnaya kimberlite, central Siberia, *Earth Planet. Sci. Lett.*, *359–360*, 206–218.
Falloon, T. J., D. H. Green, L. V. Danyushevsky and A. W. McNeill (2008), The composition of near-solidus partial melts of fertile peridotite at 1 and 1.5 GPa: Implications for the petrogenesis of MORB, *J. Petrol.*, *49*, 591–613.
Fan, J., and R. Kerrich (1997), Geochemical characteristics of aluminum depleted and undepleted komatiites and HREE-enriched low-Ti tholeiites, *Western Abitibi greenstone belt: A heterogeneous mantle plume-convergent margin environment. Geochim. Cosmochim. Acta*, *61*, 4723–4744.
Fitton, G. J., and M. Godard (2004), Origin and evolution of magmas on the Ontong Java Plateau, in *Origin and Evolution of the Ontong Java Plateau, Geol. Soc. Spec. Pub., 229*, edited by J. G. Fitton, et al., pp. 151–178, The Geological Society, London, U. K.
Ford, C. E., D. G. Russell, J. A. Craven, and M. R. Fisk (1983), Olivine-liquid equilibria: Temperature, pressure and composition dependence of the crystal/liquid cation partition coefficients for Mg, Fe^{2+}, Ca and Mn, *J. Petrol.*,*24*, 256–265.
Ghiorso, M. S. (1994), Algorithms for the estimation of phase stability in heterogeneous thermodynamic systems, *Geochim. Cosmochim. Acta 58*, 5489–5501.
Ghiorso, M. S., and R. O. Sack (1995), Chemical mass transfer in magmatic processes IV. A revised and internally consistent thermodynamic model for the interpolation and extrapolation of liquid-solid equilibria in magmatic systems at elevated temperatures and pressures, *Contrib. Mineral. Petrol.*, *119*, 197–212.
Ghiorso, M. S., M. M. Hirschmann, P. W. Reiners and V. C. Kress III (2002), The pMELTS: A revision of MELTS for improved calculation of phase relations and major element partitioning related to partial melting of the mantle to 3 GPa, *Geochem. Geophys. Geosyst.*, *3*(5), 1030, doi: 10.1029/2001GC000217.
Herzberg, C. T. (1992), Depth and degree of melting of komatiites, *J. Geophys. Res. 97*, 4521–4540.
Herzberg, C. (2004), Geodynamic information in peridotite petrology, *J. Petrol. 45*, 2507–2530.
Herzberg, C. (2006), Petrology and thermal structure of the Hawaiian plume from Mauna Kea volcano, *Nature*, *444*, 605–609.
Herzberg, C. (2011), Identification of Source Lithology in the Hawaiian and Canary Islands: Implications for Origins, *J. Petrol.*, *52*, 113–146.
Herzberg, C., and J. Zhang (1996), Melting experiments on anhydrous peridotite KLB-1: Compositions of magmas in the upper mantle and transition zone, *J. Geophys. Res.*, *101*, 8271–8295.
Herzberg, C., and P. D. Asimow (2008), Petrology of some oceanic island basalts: PRIMELT2.XLS software for primary magma calculation, *Geochem. Geophys. Geosyst.*, *8*, Q09001, doi:10.1029/2008GC002057.
Herzberg, C., and E. Gazel (2009), Petrological evidence for secular cooling in mantle plumes, *Nature*, *458*, 619–622.
Herzberg, C. and M. J. O'Hara (2002), Plume-associated ultramafic magmas of Phanerozoic age, *J. Petrol.*, *43*, 1857–1883.
Herzberg, C., P. Raterron, and J. Zhang (2000), New experimental observations on the anhydrous solidus for peridotite KLB-1, *Geochem. Geophys. Geosyst.*, *1*(11), 1051, doi:10.1029/2000GC000089.
Herzberg C., P. D. Asimow, N. Arndt, Y. Niu, C. M. Lesher, J. G. Fitton, M. J. Cheadle, and A. D. Saunders (2007), Temperatures in ambient mantle and plumes: Constraints from basalts, picrites and komatiites, *Geochem. Geophys. Geosyst. 8*, Q02006, doi:10.1029/2006GC001390.
Herzberg, C., K. Condie, and J. Korenaga (2010), Thermal history of the Earth and its petrological expression, *Earth Planet. Sci. Lett.*, *292*, 79–88.
Herzberg, C., R. A. Cabral, M. D. Jackson, C. Vidito, J. M. D. Day, and E. Hauri (2014), Phantom Archean crust in Mangaia hotspot lavas and the meaning of heterogeneous mantle, *Earth Planet. Sci. Lett.*, *396*, 97–106.
Herzberg, C. T. (1992), Depth and degree of melting of komatiites, *J. Geophys. Res*, *97*, 4521–4540.
Hirose, K., and I. Kushiro (1993), Partial melting of dry peridotites at high pressures: Determination of compositions of melts segregated from peridotite using aggregates of diamond, *Earth Planet. Sci. Lett.*, *114*, 477–489.
Hirschmann, M. M. (2000), Mantle solidus: Experimental constraints and the effects of peridotite composition, *Geochem. Geophys. Geosyst.*, *1*(10), 1042, doi:10.1029/2000GC000070.
Holland, T. J. B., N. F. C. Hudson, R. Powell, and B. Harte (2013), New thermodynamic models and calculated phase equilibria in NCFMAS for basic and ultrabasic compositions through the transition zone into the uppermost lower mantle, *J. Petrol.*, *54*, 1901–1920.
Iwamori, H., D. McKenzie, and E. Takahashi (1995), Melt generation by isentropic mantle upwelling, *Earth Planet. Sci. Lett.*, *134*, 253–266.
Katsura, T., A. Yoneda, D. Yamazaki, T. Yoshino, and E. Ito (2010), Adiabatic temperature profile in the mantle, *Phys. Earth Planet Inter.*, *183*, 212–218.
Kimura, J.-I., and A. A. Ariskin (2014), Calculation of water-bearing primary basalt and estimation of source mantle conditions beneath arcs: PRIMACALC2 model for WINDOWS, *Geochem. Geophys. Geosyst.*, *15*, 1494–1514, doi:10.1002/2014GC005329.
Kimura, J.-I., B. R., Hacker, P. E. van Keken, H. Kawabata, T. Yoshida, and R. J. Stern (2009), Arc Basalt Simulator version 2, a simulation for slab dehydration and fluid-fluxed mantle melting for arc basalts: Modeling scheme and application, *Geochem. Geophys. Geosyst.*, *10*, Q09004, doi:10.1029/2008GC002217.
Langmuir, C. H., and G. N. Hanson (1980), An evaluation of major element heterogeneity in the mantle sources of basalts, *Philos. Trans. R. Soc. London A*, *297*, 383–407.
Langmuir, C. H., E. M. Klein, and T. Plank (1992), Petrological systematics of Mid-Ocean Ridge Basalts: Constraints on melt generation beneath ocean ridges, in *Mantle Flow and Melt Generation at Mid-Ocean Ridges, Geophys. Monogr. Ser.*, vol. 71, edited by J. P. Morgan, D. K. Blackman, and J. M. Sinton, pp. 183–280, AGU, Washington, D. C.

Laporte, D., S. Lambart, P. Schiano, and L. Ottolini (2014), Experimental derivation of nephenline syenite and phonolite liquids by partial melting of upper mantle peridotites, *Earth Planet. Sci. Lett.*, *404*, 319–331.
Larsen, L. M., and A. K. Pedersen (2009), Processes in high-Mg, high T magmas: Evidence from olivine, chromite and glass in Paleogene picrites from West Greenland, *J. Petrol.*, *41*, 1071–1098.
Lee, C.-T., and E. J. Chin (2014), Calculating melting temperatures and pressures of peridotite protoliths: Implications for the origin of cratonic mantle, *Earth Planet. Sci. Lett.*, *403*, 273–286.
Lee, C.-T., P. Luffi, T. Plank, H. Dalton, and W. P. Leeman (2009), Constraints on the depths and temperatures of basaltic magma generation on Earth and other terrestrial planets using new thermobarometers for mafic magmas, *Earth Planet. Sci. Lett.*, *279*, 20–33.
Lesher, C. E., J. Pickering-Witter, G. Baxter and M. Walter (2003), Melting of garnet peridotite: Effects of capsules and thermocouples, and implications for the high-pressure solidus, *Am. Mineral.*, *88*, 1181–1189.
Longhi, J. (2002), Some phase equilibrium systematics of lherzolite melting: I, *Geochem. Geophys. Geosyst.*, *3*(3), 1020, doi:10.1029/2001GC000204.
McDonough, W. F., and S.-s. Sun (1995), The composition of the Earth, *Chem. Geol.*, *120*, 223–253.
McKenzie, D. (1984), The generation and compaction of partial melts, *J. Petrol.*, *25*, 713–765.
McKenzie, D., and M. J. Bickle (1988), The volume and composition of melt generated by extension of the lithosphere, *J. Petrol.*, *29*, 625–679.
O'Hara, M. J. (1968), Are ocean floor basalts primary magmas?, *Nature*, *220*, 683–686.
Ohtani, E., and M. Kumazawa (1981), Melting of forsterite (Mg_2SiO_4) up to 15 GPa, *Phys. Earth Planet. Inter.*, *27*, 32–38.
Presnall, D. C. and M. J. Walter (1993), Melting of forsterite, Mg_2SiO_4 from 9.7 to 16.5 GPa, *J. Geophys. Res.*, *98*, 19,777–19,783.
Puchtel, I. S., M. Humayun, A. J. Campbell, R. A. Sproule, and C. M. Lesher (2004), Platinum group element geochemistry of komatiites from the Alexo and Pyke Hill areas, Ontario, Canada, *Geochim. Cosmochim. Acta*, *68*, 1361–1383.
Putirka, K. D., M. Perfit, F. J. Ryerson, and M. G. Jackson (2007), Ambient and excess mantle temperatures, olivine thermometry, and active vs. passive upwelling, *Chem. Geol.*, *241*, 177–206.
Robinson, J. A. C., B. J. Wood, and J. D. Blundy (1998), The beginning of melting of fertile and depleted peridotite at 1.5 GPa, *Earth Planet. Sci. Lett.*, *155*, 97–111.
Sinton, J., K. Grönvold, and K. Sæmundsson (2005), Postglacial eruptive history of the Western Volcanic Zone, Iceland, *Geochem. Geophys. Geosyst.*, *6*, Q12009, doi:10.1029/2005GC001021.
Smith, P. M., and P. D. Asimow (2005), Adiabat_1ph: A new public front-end to the MELTS, pMELTS, and pHMELTS models, *Geochem. Geophys. Geosyst.*, *6*, Q02004, doi:10.1029/2004GC000816.
Stolper, E. M., S. B. Sherman, M. O. Garcia, M. B. Baker, and C. Seaman (2004), Glass in the submarine section of the HSDP2 drill core, Hilo, Hawaii, *Geochem. Geophys. Geosyst.*, *5*, Q07G15, doi:10.1029/2003GC000553.
Sugawara, T. (2000), Empirical relationships between temperature, pressure, and MgO content in olivine and pyroxene saturated liquid, *J. Geophys. Res.*, *105*, 8457–8472.
Takahashi, E. (1986), Melting of a dry peridotite KLB-1 up to 14 GPa: Implications on the origin of peridotitic upper mantle, *J. Geophys. Res.*, *91*, 9367–9382.
Takahashi, E., T. Shimazaki, Y. Tsuzaki, and H. Yoshida (1993), Melting study of a peridotite KLB-1 to 6.5 GPa, and the origin of basaltic magmas, *Philos. Trans. R. Soc. London A*, *342*, 105–120.
Till, C. B., T. L. Grove, and M. J. Krawczynski (2012), A melting model for variably depleted and enriched lherzolite in the plagioclase and spinel stability fields, *J. Geophys. Res.*, *117*, B06206, doi:10.1029/2011JB009044.
Toplis, M. J. (2005), The thermodynamics of iron and magnesium partitioning between olivine and liquid: Criteria for assessing and predicting equilibrium in natural and experimental systems, *Contrib. Mineral. Petrol.*, *149*, 22–39.
Walter, M. J. (1998), Melting of garnet peridotite and the origin of komatiite and depleted lithosphere, *J. Petrol.*, *39*, 29–60.